Journal of Applied Polymer Science

# Preparation of zirconia loaded poly(acrylate) antistatic hard coatings on PMMA substrates

**Chao-Ching Chang,[1,2] Chin-Yuan Hsieh,[1] Feng-Hsi Huang,[1] Liao-Ping Cheng[1,2]**
[1]Department of Chemical and Materials Engineering, Tamkang University, Taipei, Taiwan
[2]Energy and Opto-Electronic Materials Research Center, Tamkang University, Taipei, Taiwan
Correspondence to: L.-P. Cheng (E-mail: lpcheng@mail.tku.edu.tw)

**ABSTRACT:** Zirconia ($ZrO_2$) nanoparticles were synthesized by hydrolysis and condensation of zirconium-*n*-propoxide (ZNP) in 1-propanol at the presence of methacrylic acid (MA), serving as a chelating agent for ZNP. The formed nanoparticles were chemically modified by the UV-curable coupling agent, 3-(trimethoxysilyl)propyl methacrylate (MSMA). The modified particles were then crosslinked with the hexa-functional monomer, dipentaerythritol hexaacrylate (DPHA), to produce transparent antistatic hard coatings on poly(methyl methacrylate) (PMMA) substrates. Sizes of the modified particles, as determined by the dynamic light scattering technique, fell over a small range of 2–20 nm. Chemical analyses of the particles and the coatings were performed using FTIR and/or solid $^{29}$SiNMR spectroscopy. Surface resistivities of the coatings were measured, and the results indicated that with inclusion of 10 wt % modified zirconia, surface resistivity of $\sim 10^9$ Ω/sq could be achieved, which amounted to ~6 order magnitude lower than that of the particle-free polymeric binder. Furthermore, this antistatic coating was very hard with pencil hardness of 8–9H, and attached perfectly to the PMMA substrate according to the peel test. © 2015 Wiley Periodicals, Inc. J. Appl. Polym. Sci. **2015**, *132*, 42411.

**KEYWORDS:** coatings; composites; nanoparticles; nanowires and nanocrystals; structure-property

Received 10 February 2015; accepted 22 April 2015
**DOI: 10.1002/app.42411**

## INTRODUCTION

Electrostatic charges are prone to accumulate on the surface of insulators, such as plastics, fabrics, and glasses. Statically charged surfaces tend to attract dirt and microorganisms, which not only causes aesthetic loss of finished surface but also engenders hygienic problems. On the other hand, when electrostatic discharge (ESD) occurs, such as by contacting a conductor, the electronic devices of an instrument could be damaged. Several ESD can even enflame volatile substances and result in explosion.[1] There are a number of approaches to reduce electrostatic charge accumulation on plastic materials. Among them applying a thin layer of antistatic coating on the surface is one of practical significance, because it is cost-effective, easy to process, and can offer additional functionalities, such as protection, self-cleaning, decoration, etc., to the plastic substrate.[2–15]

$ZrO_2$ has been reported to be useful for producing antistatic coatings; as it improved significantly the mechanical strength (e.g., hardness and anti-abrasiveness) of the coatings, in addition to dissipating static changes.[2] Preparation and modification of $ZrO_2$ nanoparticles by the sol–gel process have been well documented.[16–27] For example, Delattre demonstrated the initial formation and subsequent cleavage of Si−O−Zr bonds during synthesis of zirconia–MPS hybrids by means of $^{29}$Si- and $^{17}$O-NMR spectroscopy.[11] Haas *et al.* prepared antistatic coatings using MSMA-functionalized $ZrO_2$ as the *host* and ionic silane as static dissipation enhancer.[2] Schmidt combined sol–gel and solvothermal processes to prepare crystalline $ZrO_2$ particles, and found that much higher tetragonal phase could be obtained for particles previously modified by MPTS in the sol–gel step.[25]

In our previous article, $ZrO_2$ nanoparticles chemically modified by the coupling agent, 3-(trimethoxysilyl)propyl methacrylate (MSMA), were synthesized and introduced into a coating formulation to prepare antistatic hard coatings.[15] Due to the bridging activity of MSMA, the nanoparticles (MSMA–$ZrO_2$) could be uniformly dispersed in the crosslinked organic matrix of dipentaerythritol hexaacrylate (DPHA). While good static dissipation could be achieved with incorporation of ~10 wt % MSMA–ZrO, there was, however, one shortage in this work that merited reinvestigation; viz., many of the prepared coating sols were unstable, which would gel quickly (typically from a few minimums to several hours) if not coated and cured soon after preparation. To solve this problem, we adopted the method of Haas *et al.*[2] and Nakayama *et al.*[28] using the chelating agent, methacrylic acid (MA), as a stabilizer during the synthesis of MSMA–ZrO. Because MA contains a C=C bond, it could be covalently linked to the polymeric network of DPHA during

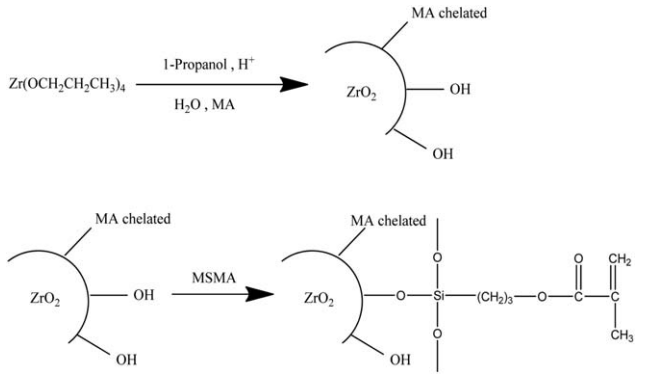


**Figure 1.** Synthesis route of the surface-modified $ZrO_2$ sol.

UV-curing of the coating. Hence, in addition to serving as a chelating agent for nano-zirconia, MA also played the role of coupling organic and inorganic moieties just like MSMA.[29] Some of the prepared coatings were highly transparent, very hard (8–9H), and static dissipative (surface resistivity $\sim 10^9$ Ω/sq). The detailed preparation and characterization of the nanocomposite coatings are presented in the sections that follow.

## EXPERIMENTAL

### Materials

Zirconium (IV) propoxide (ZNP, 70% in propanol) and 3-(trimethoxysilyl)propyl methacrylate (MSMA, 98%) were purchased from Aldrich. Methacrylic acid (MA, 98%) and 1-propanol (99.5%) were purchased from Fluka. Nitric acid (60% in water) was purchased from Showa. The multi-functional crosslinking agent, dipentaerythritol hexaacrylate (DPHA) was purchased from Toagosei (M-402). The photoinitiator, 2-hydroxy-2-methyl-1-phenyl-1-propanone (HMPP, Darocure 1173) was supplied by Ciba-Geigy. All materials were used as received.

### Synthesis of Organically Modified $ZrO_2$

ZNP was mixed with 1-propanol to form a homogeneous solution. Then, MA was slowly added and the solution was stirred for 1 h to allow sufficient chelating reaction. Afterward nitric acid was added to induce the sol–gel reaction, which was continued for 3 h at room temperature, see Figure 1. To the formed $ZrO_2$ sol, MSMA was slowly dropt using a syringe pump. After 3 h of reaction, additional nitric acid was added to ensure complete hydrolysis and condensation of MSMA, which was carried out for another 3 h. The produced colloidal particles are called $MSZrO_2$ hereinafter, and the compositions of various chemical species used for the above synthetic process are summarized in Table I.

### Synthesis of Antistatic Coatings

UV-sensitive coating sols were prepared by adding DPHA, Darocure 1173, and additional 1-propanol to the $MSZrO_2$ sol with a solid content adjusted to 25 wt % and an inorganic content to 10 wt % (theoretical). The prepared coating sols were coated using doctor-blade (applicator with 150 μm gap) on poly(-methyl methacrylate) (PMMA) substrates, and then prebaked at 80°C for 30 s, followed by UV irradiation with a conventional medium-pressure mercury lamp (broadband, ~1000 mJ/cm$^2$).[29–32] Then, the samples were postbaked at 100°C for 3 h to remove residual trapped solvents. Thick self-supported films (1–2 mm in thickness) were also prepared for thermal analyses, for which the coating sols were poured in Teflon molds, UV-cured, and then postbaked as usual. In a few cases, where surface electric resistivity measurement was required, a mixture of poly(ethylene glycol diacrylate) (PEGDA) (28 wt %) and DPHA (72 wt %) instead of pure DPHA was used as the curing agent to reduce the brittleness of the films. These samples were cured on the Teflon plates with the curing and heating procedures described above.

### Characterization

**FTIR Analysis.** FTIR spectra of the synthesized sols were taken using a Nicolet 550 spectrometer. Samples were cast on KBr discs and baked, and the spectra were collected over the wavenumber range of 400–4000 cm$^{-1}$, with a resolution of 4 cm$^{-1}$.

**NMR Analysis.** Solid-state $^{29}$Si-NMR spectra of UV-cured coatings were recorded on a Bruker DSX400 WB spectrometer at 79.49 MHz. The sample, in the form of fine powder, was subjected to magic angle spinning at the rate of 5 kHz. The pulse widths and recycle delays were set to 12 μs and 2 s, respectively. The chemical shifts were expressed in ppm with respect to tetramethylsilane.

**DLS Analysis.** The size and size distribution of $MSZrO_2$ in the sol were determined by dynamic light scattering (DLS) method, using a Malvern DTS 3000HS Zetasizer at 25°C. A 4 mL sol sample at the concentration of 0.5 wt % was injected into the quartz cuvette secured on the holder, and the scattered light was recorded at 173° with respect to the source beam.

**Table I.** Molar Ratio of the Components for Synthesis of Surface Modified $ZrO_2$

| | | | | $HNO_3$ | | $H_2O$ | | |
|---|---|---|---|---|---|---|---|---|
| Sample | ZNP | MA | MSMA | 1st | 2nd | 1st | 2nd | 1-Propanol |
| ZM1 | 1 | 0.2 | 0 | 0.51 | 0 | 2 | 0 | 25.2 |
| ZM2 | 1 | 0.5 | 0 | 0.51 | 0 | 2 | 0 | 25.2 |
| ZM3 | 1 | 1 | 0 | 0.51 | 0 | 2 | 0 | 25.2 |
| ZMS1 | 1 | 0.5 | 0.2 | 0.51 | 0.1 | 2 | 0.4 | 25.2 |
| ZMS3 | 1 | 0.5 | 0.5 | 0.51 | 0.26 | 2 | 1 | 25.2 |
| ZMS5 | 1 | 0.5 | 1.0 | 0.51 | 0.51 | 2 | 2 | 25.2 |
| ZMS3-2 | 1 | 0.2 | 0.5 | 0.51 | 0.26 | 2 | 1 | 25.2 |

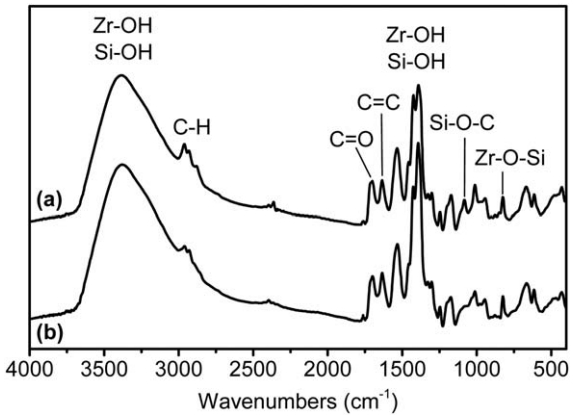


**Figure 2.** FTIR spectrum of ZMS3: (a) 3 h after addition of MSMA, and (b) 3 h after addition of additional nitric acid.

**SEM Image.** Morphology of the UV-cured coating was observed using a field emission scanning electron microscope (FESEM, LEO 1530, Carl Zeiss). The sample was vacuum-dried and then fractured in liquid nitrogen to expose the cross section. It was attached to a holder by conductive copper tapes. Silver pastes were applied at the edges, and then it was sputtered with a thin layer (~1.0 nm) of Pt–Pd alloy to enhance electronic conductivity. The image was taken under the acceleration voltage of 15 kV via an in-lens detector.

**TGA Analysis.** Thermal gravimetric analyzer (TGA, Hi-Res TGA 2950 from TA Instruments) was used to measure the thermal decomposition temperature ($T_d$) of the cured coatings. Samples (10–15 mg) were heated from room temperature to 600°C with a heating rate of 20°C/min under nitrogen flow.

**Adhesion Analysis.** Peel tests (ASTM D3359) were carried out to evaluate the adhesion strengths of coatings cured on PMMA substrates. The degree of adhesion was recorded as the percentage of the residual film on the substrate after peeling by standard tapes (3M-610).

**Hardness Analysis.** The hardness (ASTM D3363) of the cured coatings was examined by the widely used pencil hardness test, using pencils of different hardness at the load of 750 g.

**Surface Electric Resistivity.** The surface electric resistivity (ASTM D257) of the cured antistatic film was measured using a HIOKI SM-8200 megohmmeter and an SM-8310 plate electrode at 1 kV and 60 s electrification time.

## RESULTS AND DISCUSSION

### Analyses of Chemical Structure by FTIR and $^{29}$Si-NMR

Comparing spectra (a) and (b), it can be seen that the Zr—O—Si signal (850 $cm^{-1}$) decreases after addition of extra nitric acid solution; that is, dissociation of the Zr—O—Si bonds has occurred during this stage of reaction.[12,13] A similar result has been reported by Delattre *et al.* based on $^{29}$Si- and $^{17}$O-NMR analyses. They also found that new Zr—O—Zr and Si—O—Si bonds were formed along with the de-bonding reaction.[13]

Figure 2 shows the spectra of a typical $MSZrO_2$ (ZMS3). Spectrum (a) depicts the case at 3 h after addition of MSMA to the $ZrO_2$ sol (second stage in Figure 1), while spectrum (b) stands for 3 h after addition of extra nitric to the $MSZrO_2$ sol. The characteristic bands, such as 2950, 1700, 1634, and 1087 $cm^{-1}$

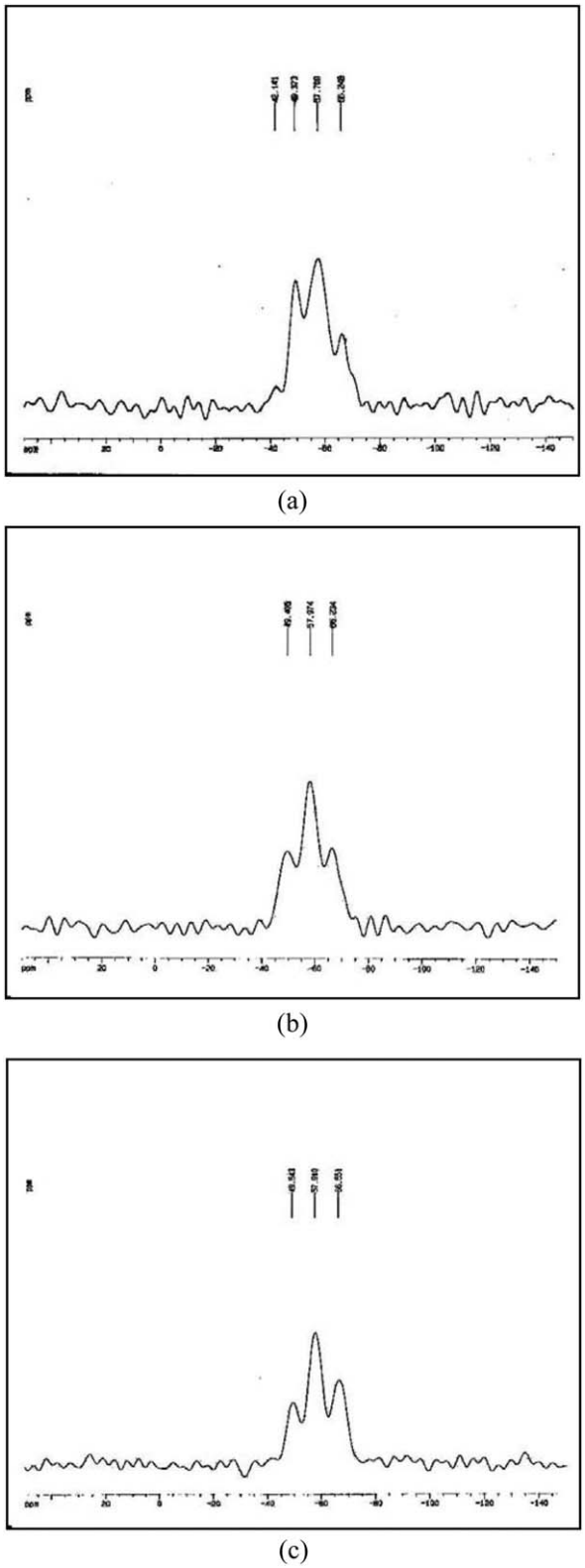


**Figure 3.** Solid-state $^{29}$Si-NMR spectra of (a) ZMS1, (b) ZMS3, and (c) ZMS3-2.

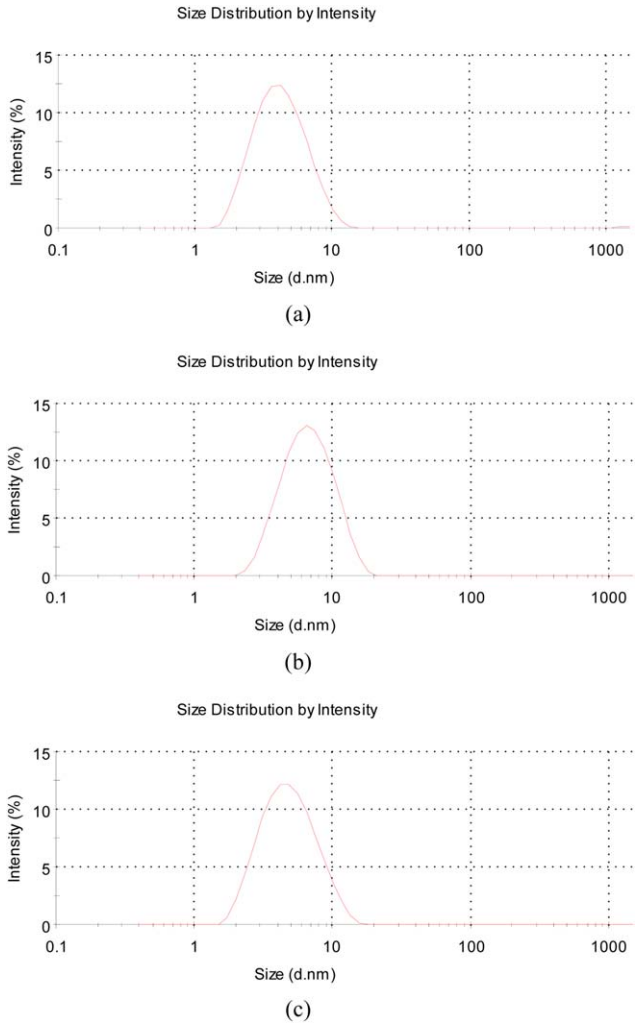


**Figure 4.** Particle size distribution of modified $ZrO_2$ in synthesized sols. (a) MA chelated $ZrO_2$, ZNP : MA = 1 : 0.5; (b) ZMS3 at 3 h after addition of MSMA; (c) ZMS3 at 3 h after addition of extra nitric acid. [Color figure can be viewed in the online issue, which is available at wileyonlinelibrary.com.]

for C—H, C=O, C=C, and Si—O—C in MSMA and MA moieties, 3400 (broad) and 1375 $cm^{-1}$ for hydroxyl of Zr—OH, and Si—OH are all clearly manifested. These bands resemble those found in the spectra of MSMA–$ZrO_2$ particles synthesized without using chelating agent.[15] Presence of MA is evidenced by the strong signal appearing at 1550 $cm^{-1}$. The absorption band due to C=O vibrations in MA are located at 1700 $cm^{-1}$ shifted to 1550 $cm^{-1}$ as MA was chelated on ZNP, consistent with the results reported by Schmidt.[33] Comparing spectra (a) and (b), it can be seen that the intensities of the C—H and Si—O—C vibrations decrease substantially after addition of extra nitric acid, and it suggests that the Si—O—$CH_3$ bond undergoes hydrolysis to form Si—OH or Si—O—Si. The solid $^{29}$Si-NMR spectra of modified $ZrO_2$ samples ZMS1, ZMS3, and ZMS3-2 are shown in Figure 3. For these samples, there can be identified three significant peaks with chemical shifts −49, −58, −67 ppm, corresponding to $T^1$ ($(HO)_2$**Si**(—O—Si≡)), $T^2$ ((HO)**Si**(—O—Si≡)$_2$), and $T^3$ (**Si**(—O—Si≡)$_3$) species of bonded MSMA.[34] The strong $T^2$ signal indicates that MSMA has undergone substantial condensation during the sol–gel process. Comparing ZMS3 and ZMS3-2, the intensities of $T^2$ and $T^3$ with respect to $T^1$ are both higher for ZMS3-2 than for ZMS3, which is consistent with the fact that ZMS3-2 has a lower MA content and thus zirconia was less chelated. On the other hand, by comparing ZMS1 and ZMS3, one finds that ZMS1 has a higher $T^1$ intensity than ZMS3 does. Since a larger amount of MSMA was added in ZMS3, it is expected that more $T^1$ species will be converted to $T^2$ or $T^3$ by condensation in this sample.

### Particle Size and Particle Size Distribution

The size and size distribution of $ZrO_2$ particles in the sol for various synthetic stages (Figure 1) were measured by the DLS technique. Figure 4 demonstrates the results of a typical example, ZMS3, in terms of scattering intensity profiles. Figure 4(a) shows that at the end of the 1st stage, the formed $MZrO_2$ particles have their sizes distributed over a relatively small range, 1.4–15 nm, with the maximum intensity located at ~4 nm. In contrast, if $ZrO_2$ were synthesized without being chelated by MA, a wider size distribution of 2–30 nm would be obtained, as shown previously.[15] At the second synthetic stage, it was intended to bind MSMA to the as-formed $MZrO_2$. As shown in Figure 4(b), the size (at intensity maximum) of the $MSZrO_2$ particles increases to ~7 nm after 3 h of reaction. Such increment is due to the attachment of various MSMA species ($T^1$, $T^2$, and $T^3$). Additional nitric acid was added to complete the reaction of MSMA. As shown in Figure 4(c), the size of the $MSZrO_2$ particles fell down to ~5 nm, for which further condensation of Zr—O—Si and Sr—O—Si was suggested.

Morphologies of the cured antistatic coatings were observed using FESEM. Figure 5 shows the high resolution cross sectional image of the sample, AZMS3 (see Table III). Some elongated crack marks appeared, which were resulted from fracturing the sample in liquid nitrogen. Other than these marks, the cross section is uniform and free of aggregated domains of particulate objects under the resolution of ca. 20 nm. This suggests that colloidal $MSZrO_2$ sol and DPHA were well mixed, and after UV curing they formed an organic/inorganic nanocomposite without appreciable phase separation via the coupling of MSMA.

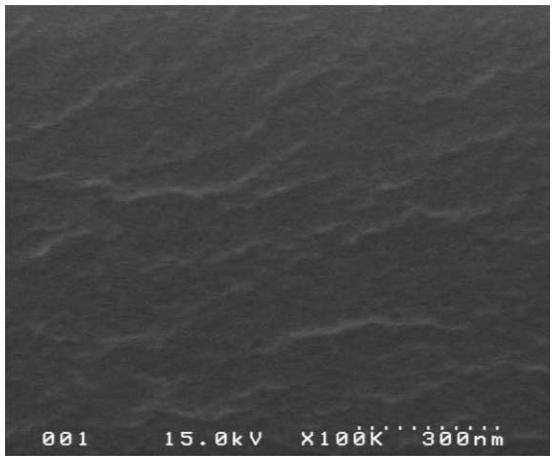


**Figure 5.** SEM micrograph of the cross section of coating AZMS3.

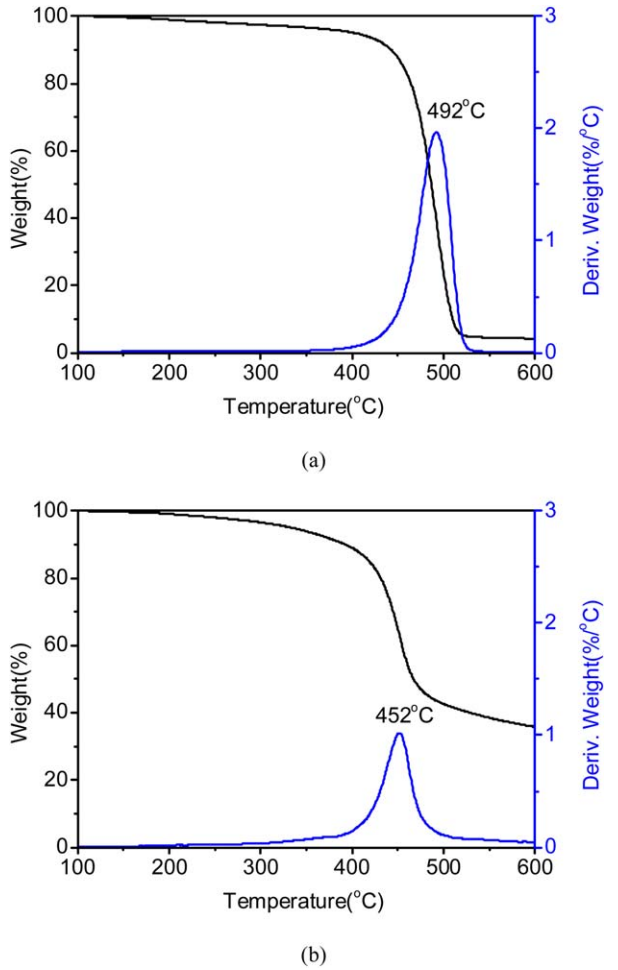


**Figure 6.** TGA thermograms of (a) poly(DPHA) and (b) AZMS3. [Color figure can be viewed in the online issue, which is available at wileyonlinelibrary.com.]

### Thermal Degradation

TGA experiments were carried out for UV-cured DPHA polymer (termed poly(DPHA), hereinafter) and various composite samples. Some representative thermograms are shown in Figure 6, and the determined decomposition temperatures at 5% weight loss ($T_d$) and at maximum rate ($T_{d,max}$) are summarized in Table II together with the char yield data. Figure 6(a) shows that poly(DPHA) underwent typical one-stage degradation behavior with $T_d$, and $T_{d,max}$ located at 401 and 492°C, respectively; beyond 530°C only limited weight loss was detected, leading to a final char yield of 4 wt %. As an example, thermograms of the composite AZMS3 (10 wt % ZMS3) are shown in Figure 6(b). One-stage degradation is also indicated; however, with $T_d = 333$°C and $T_{d,max} = 452$°C much lower than those of poly(DPHA). Thermal degradation data of the sample AZS3 [MSMA-modified $ZrO_2$ without MA, see Ref. (15)] are also given in Table II. The $T_d$ and $T_{d,max}$ are close to those of AZMS3. Since MSMA moiety would not lower the degradation point of poly(DPHA),[32] it is reasonable to propose that $ZrO_2$ was the major species that caused the unexpected early degradation of poly(DPHA). Table II further indicated that samples containing higher amounts of ZMS3 degraded earlier, which strengthened the argument that $ZrO_2$ have assisted in bond dissociation of poly(DPHA). The bond dissociation mechanism, however, required further investigation.

**Table II.** Thermal Decomposition Temperature and Char Yield of ZMS3 and ZS3 Nanocomposites with Various Inorganic Contents

| ZMS3 (wt %) | $T_d$ (°C) | $T_{d,max}$ (°C) | Char yield (%) |
|---|---|---|---|
| 0 | 401 | 492 | 4.2 |
| 0.5 | 384 | 469 | 13.6 |
| 1.0 | 381 | 466 | 16.4 |
| 3.0 | 380 | 461 | 21.1 |
| 10 | 333 | 452 | 35.8 |
| 10[a] | 334 | 459 | 32.2 |

[a] ZS3 is MSMA-modified $ZrO_2$ prepared without using MA, cf. Ref. (15).

**Table III.** Hardness and Surface Resistivity of Prepared Coatings

| Sample code | Hardness | Adhesion (%) | Surface resistivity[a] (Ω/sq) |
|---|---|---|---|
| AZM1 | - | <50 | - |
| AZM2 | 8H | 100 | - |
| AZM3 | 8H | 100 | - |
| AZMS1 | 8H | 100 | - |
| AZMS3 | 9H | 100 | $5.7 \times 10^{11}$ |
| AZMS3[b] | 8H | 100 | $8.4 \times 10^{10}$ |
| AZMS5 | 7H | 100 | - |
| AZMS3-2 | 8H | 100 | $4.3 \times 10^{9}$ |
| AZMS3-2[b] | 8H | 100 | $3.3 \times 10^{9}$ |
| CA80-1% | | | $9.2 \times 10^{9}$ |
| CA80-3% | | | $1.55 \times 10^{9}$ |
| CA80-5% | | | $1.38 \times 10^{9}$ |

[a] PEGDA + DPHA mixture was used as the binder.
[b] 20 wt % inorganic content.

### Adhesion, Hardness, and Antistatic Tests

The pencil hardness of the films coated on PMMA substrates was examined and the results are listed in Table III. Poly(DPHA) exhibited high hardness of 7H, confirming that a robust network structure had been built via UV-curing of the hexa-functional monomer DPHA. Incorporation of $ZrO_2$ particles reinforced the polymer and gave even higher hardness, 8–9H. Specifically, the hardness of AZMS3 reached 9H (highest measurable pencil hardness) just by incorporation of 10 wt % modified $ZrO_2$.

It is noted that all coatings, except for AZM1 with lower level of surface modification, exhibited 100% adhesion according to the tape tests. This suggests that the $ZrO_2$ particles could be well dispersed in the polymer host, if they were properly organically modified. For the exceptional sample (AZM1), phase separation has occurred due to insufficient coupling between $ZrO_2$ and DPHA, and the aggregated inorganic particles have also deteriorated their adherence to the substrate.

The static dissipative capabilities of the cured coatings were evaluated by means of surface electrical resistivity measurements. The results of some typical samples are shown in Table III. The cross-linked DPHA–PEGDA copolymer had very high surface resistivity of $2 \times 10^{15}$ Ω/sq, a value typical of polymeric insulators. As 10 wt % of $MSZrO_2$ was loaded, the resistivity of the coatings decreased considerably to the antistatic level, $<10^{12}$ Ω/sq. The resistivity of AZMS3-2 was lower than that of AZMS3, consistent with the fact that the latter contained higher amount of organic species on the particle surface. Also, increasing the $MSZrO_2$ content to 20 wt % resulted in lower resistivity. The surface resistivity of the coating loaded with 5 wt % of commercial antistatic regent, CA80, was $1.38 \times 10^9$ Ω/sq,[15] only slightly lower than AZM7. Further increase of CA80 dosage leaded to phase separations, which downgraded the optical and mechanical properties of the coatings. Therefore, $ZrO_2$/poly(acrylate) hard coatings developed in the present research have potentials in antistatic applications.

## CONCLUSION

MSMA, serving as a coupling agent, was covalently boned to $ZrO_2$ synthesized by an acid catalyzed sol–gel process with the aid of the chelating agent MA. FTIR analyses confirmed the presence of Zr—O—Si in the formed particles; however, this bond would dissociate later if extra nitric acid solution were added during synthesis. The synthesized UV-sensitive particles (~7 nm) were cured with the hexa-functional crosslinker, DPHA, to yield hard coatings that exhibited static dissipative capability on PMMA substrates. FESEM imaging of the coatings confirmed that the organically modified $ZrO_2$ nano-particles were well dispersed in the cured polymeric binder without aggregated phases up to the resolution of ~20 nm. The antistatic performances of various coatings were examined, and in the optimal case, surface resistivity as low as $3.3 \times 10^9$ Ω/sq were achieved, being ~6 order of magnitude lower than that of the binder polymer. In addition, the pencil hardness of this coating reached 8H, and according to the peel test, the coating adhered 100% to the PMMA surface.

## ACKNOWLEDGMENTS

The authors thank the Ministry of Science and Technology of Taiwan for the final support (NSC 96–2628–E–032–001–MY3).

## REFERENCES

1. Rosner, R. B. *IEEE Trans. Device Mater. Reliab.* **2001**, *1*, 9.
2. Haas, K. H.; Amberg-Schwab, S.; Rose, K. *Thin Solid Films* **1999**, *351*, 198.
3. Al-Dahoudi, N.; Bisht, H.; Göbbert, C.; Krajewski, T.; Aegerter, M. A. *Thin Solid Films* **2001**, *392*, 299.
4. Al-Dahoudi, N.; Aegerter, M. A. *Mol. Crystallogr. Liq. Crystallogr. Sci. Technol. Sect. A* **2002**, *374*, 91.
5. Al-Dahoudi, N.; Aegerter, M. A. *J. Sol-Gel Sci. Technol.* **2003**, *26*, 693.
6. Kim, J.-Y.; Han, Y.-K.; Kim, E.-R.; Suh, K.-S. *Curr. Appl. Phys.* **2002**, *2*, 123.
7. Ohishi, T. *J. Non-Crystallogr. Solids* **2003**, *332*, 87.
8. Wouters, M. E. L.; Wolfs, D. P.; Van Der Linde, M. C.; Hovens, J. H. P.; Tinnemans, A. H. A. *Prog. Org. Coat.* **2004**, *51*, 312.
9. Currie, E. P. K.; Tilley, M. *J. Soc. Inf. Disp.* **2005**, *13*, 773.
10. Hidden, G.; Boudou, L.; Martinez-Vega, J.; Remaury, S.; Nabarra, P. *Polym. Eng. Sci.* **2006**, *46*, 1079.
11. Aegerter, M. A.; Almeida, R.; Soutar, A.; Tadanaga, K.; Yang, H. *J. Sol-Gel Sci. Technol.* **2008**, *47*, 203.
12. Castro, M. R. S.; Al-Dahoudi, N.; Oliveira, P. W.; Schmidt, H. K. *J. Nanopart. Res.* **2009**, *11*, 801.
13. Kim, J. H.; Jung, J. M.; Sultana, T.; Kwak, J. Y.; Hwang, T. K.; Lim, K. T. *Mol. Crystallogr. Liq. Crystallogr.* **2010**, *532*, 83.
14. Chiu, H.-T.; Chang, C.-Y.; Chen, C.-L.; Chiang, T.-Y.; Guo, M.-T. *J. Appl. Polym. Sci.* **2011**, *120*, 202.
15. Chang, C.-C.; Hwang, F.-H.; Hsieh, C.-Y.; Chen, C.-C.; Cheng, L.-P. *J. Coat. Technol. Res.* **2013**, *10*, 73.
16. Delattre, L. *J. Sol-Gel Sci. Technol.* **1997**, *8*, 567.
17. Monte, F. D.; Cheben, P.; Grover, C. P.; Mackenzie, J. D. *J. Sol-Gel Sci. Technol.* **1999**, *15*, 73.
18. Zhao, J.; Fan, W.; Wu, D.; Sun, Y. *J. Non-Crystallogr. Solid* **2000**, *261*, 15.
19. Voelkel, J. *Mol. Cryst. Liq. Cryst. Sci. Technol. Sect. A* **2000**, *354*, 503.
20. Villegas, M. A. *Thin Solid Films* **2001**, *382*, 124.
21. Caracoche, M. C.; Rivas, P. C.; Cervera, M. M.; Caruso, R. B.; Benavídez, E.; Sanctis, O. *J. Mater. Res.* **2003**, *18*, 208.
22. Caruso, R.; De Sanctis, O.; Macías-García, A.; Benavidez, E.; Mintzer, S. R. *J. Mater. Process. Technol.* **2004**, *152*, 299.
23. Ehrhart, G.; Capoen, B.; Robbe, O.; Boy, Ph.; Turrell, S.; Bouazaoui, M. *Thin Solid Films* **2006**, *496*, 227.
24. Mizuno, M.; Sasaki, Y.; Lee, S.; Katakura, H. *Langmuir* **2006**, *22*, 7137.
25. Schmidt, T.; Mennig, M. *J. Am. Ceram. Soc.* **2007**, *90*, 1401.
26. Liang, L.; Xu, Y.; Wu, D.; Sun, Y. *Mater. Chem. Phys.* **2009**, *114*, 252.
27. Di Maggio, R.; Dirè, S.; Callone, E.; Girardi, F.; Kickelbick, G. *Polymer* **2010**, *51*, 832.
28. Nakayama, N.; Hayashi, T. *Compos. Part A* **2007**, *38*, 1996.
29. Chang, C. C.; Cheng, L. P.; Huang, F. H.; Lin, C. Y.; Hsieh, C. F.; Wang, W. H. *J. Sol-Gel Sci. Technol.* **2010**, *55*, 199.
30. Chang, C. C.; Cheng, L. P.; Lin, C.-Y.; Yu, Y.-Y. *J. Sol-Gel Sci. Technol.* **2012**, *63*, 30.
31. Chang, C. C.; Huang, F. H.; Chang, H. H.; Don, T. M.; Chen, C. C.; Cheng, L. P. *Langmuir* **2012**, *28*, 17193.
32. Chang, C. C.; Oyang, T. Y.; Chen, Y. C.; Huang, F. H.; Cheng, L. P. *J. Coat. Technol. Res.* **2014**, *11*, 381.
33. Schmidt, H. K. *J. Sol-Gel Sci. Technol.* **1997**, *8*, 557.
34. Rankin, S. E.; Macosko, C. W.; McCormick, A. V. *AIChE J.* **1998**, *44*, 1141.